SCIENTIFIC REPORTS
nature research

Check for updates

OPEN

Quantitative in vivo bioluminescence imaging of orthotopic patient-derived glioblastoma xenografts

Anna L. Koessinger[1,2,3], Dominik Koessinger[1,2,3], Katrina Stevenson[2], Catherine Cloix[1,2], Louise Mitchell[1], Colin Nixon[1], Natividad Gomez-Roman[2], Anthony J. Chalmers[2], Jim C. Norman[1,2]✉ & Stephen W. G. Tait[1,2]✉

Despite extensive research, little progress has been made in glioblastoma therapy, owing in part to a lack of adequate preclinical in vivo models to study this disease. To mitigate this, primary patient-derived cell lines, which maintain their specific stem-like phenotypes, have replaced established glioblastoma cell lines. However, due to heterogenous tumour growth inherent in glioblastoma, the use of primary cells for orthotopic in vivo studies often requires large experimental group sizes. Therefore, when using intracranial patient-derived xenograft (PDX) approaches, it is advantageous to deploy imaging techniques to monitor tumour growth and allow stratification of mice. Here we show that stable expression of near-infrared fluorescent protein (iRFP) in patient-derived glioblastoma cells enables rapid, direct non-invasive monitoring of tumour development without compromising tumour stemness or tumorigenicity. Moreover, as this approach does not depend on the use of agents like luciferin, which can cause variability due to changing bioavailability, it can be used for quantitative longitudinal monitoring of tumour growth. Notably, we show that this technique also allows quantitative assessment of tumour burden in highly invasive models spreading throughout the brain. Thus, iRFP transduction of primary patient-derived glioblastoma cells is a reliable, cost- and time-effective way to monitor heterogenous orthotopic PDX growth.

Glioblastoma is the most common malignant intrinsic brain tumour in adults[1]. Current treatment regimens, consisting of surgical resection followed by radio- and chemotherapy, have limited efficacy in combating the disease, and this is reflected in a dismal prognosis for the patients[2,3]. Improvement of therapeutic strategies is urgently needed to increase patient life expectancy and to reduce the disabling effects of the disease and its therapy. Development of novel therapies implicitly depends on reproducible and reliable models for preclinical studies in vitro and in vivo. However, experiments using orthotopic xenografts of established glioblastoma cell lines in immunocompromised mice to investigate effects of new therapies have many limitations. Most importantly, positive results observed in these preclinical studies have not been reproduced in subsequent clinical studies[4,5].

To better recapitulate human disease, the use of patient-derived glioblastoma stem-like cells (GSC) has gained increasing prominence in recent years[6,7]. Several studies have demonstrated that patient-derived GSC cultured in serum-free neurobasal medium, supplemented with epidermal growth factor (EGF) and fibroblast growth factor (FGF), are more representative of primary glioblastoma than traditional, commercially-available glioblastoma cell lines[8,9]. Nevertheless, it is not trivial to maintain the GSC population of surgical specimens using in vitro cell culture systems as stem cell growth varies due to plasticity, resulting in artificial selection of proliferating, rather than dormant GSC. Therefore, it is advantageous to study glioblastoma behaviour in vivo, as brain tissue provides the most appropriate microenvironment for maintenance of the stem signature of patient-derived xenografts (PDX)[7]. However, due to their intrinsic heterogeneity, orthotopic PDXs display a much greater range of growth rates between animal subjects compared to established glioblastoma cell lines[4,10]. Although this variability is a

[1]Cancer Research UK Beatson Institute, Garscube Estate, Glasgow G61 1BD, UK. [2]Institute of Cancer Sciences, University of Glasgow, Garscube Estate, Glasgow G61 1QH, UK. [3]These authors contributed equally: Anna L. Koessinger and Dominik Koessinger. ✉email: j.norman@beatson.gla.ac.uk; stephen.tait@glasgow.ac.uk

good reflection of the heterogeneity of the parental tumour, differences in growth characteristics, and therefore PDX size and the degree of dissemination at defined time points, lead to difficulties in quantifying and interpreting animal studies. Thus, large cohorts of animals are needed to achieve the necessary statistical power in these preclinical studies.

Currently, intra-vital bioluminescent imaging (BLI) with luciferase is commonly used to monitor xenograft growth[11]. Yet, in vivo luciferase assays are limited to descriptive analysis since factors such as fluctuating substrate access to the target tissue result in variable luciferin bioavailability in tumours. Moreover, luciferase-based BLI does not allow for absolute quantification of the same tumour over time. Although magnetic resonance imaging (MRI) is ubiquitously used as clinical standard of care to diagnose brain tumours in humans, this technique has major drawbacks in preclinical settings. First of all, small animal MRIs are not widely available. Secondly, the procedure and its analysis are expensive as well as onerous for animals, requiring prolonged episodes of anaesthesia. Thirdly, MRIs often only measure indirect indicators of tumour pathology, such as focal brain oedema, which do not necessarily reflect the size and margins of the tumour itself.

To address these challenges, we have adapted a method of viral transduction to express iRFP, a protein with excitation and emission in the near-infrared spectrum, in patient-derived GSC, whilst maintaining their stem-like phenotype, growth characteristics and individual susceptibility to drug treatments. Using these cells, we find that imaging iRFP is a reliable, rapid and cost-effective method to monitor tumour bulk and infiltrative growth of orthotopic glioblastoma models in vivo.

Materials and methods

Patient-derived GSC and Cell culture reagents. Patient-derived E2, G1 and G7 glioblastoma stem-like cells (GSC), obtained from surgical resection specimens of anonymised patients as previously described[12,13], were kindly provided by Prof. Colin Watts. Serum-free medium for GSC was Advanced Dulbecco's modified Eagle's medium F12 (Thermo Fisher Scientific), supplemented with 2 mM glutamine, 4 µg/ml heparin (Sigma), 1% B27 (Thermo Fisher Scientific), 0.5% N2 (Thermo Fisher Scientific), 20 ng/ml EGF and 10 ng/ml FGF (Thermo Fisher Scientific). GSC were cultured in a 37 °C incubator at 5% CO_2 and, when grown as monolayers, on Matrigel (Corning) pre-coated plates. For all experiments GSC were used up to ten passages after thawing. Cell lines were routinely tested for mycoplasma.

iRFP vector and retroviral transduction. As described previously, plasmids encoding iRFP IRES puro had been inserted into a pBABE vector[11]. For GSC transduction HEK293-FT cells (4×10^6 in a 10 cm dish, cultured in high-glucose DMEM, complemented with 10% FCS and 2 mM glutamine) were transfected using 4 µg polyethylenimine (PEI, Polysciences Inc., Warrington, USA) per µg plasmid DNA. The retroviral transfer vector plasmid pBABE iRFP IRES puro (kindly provided by Andreas Hock[11]), packaging plasmid HIV-gag-pol (Addgene 14887) and envelope plasmid pUVSVG (Addgene 8454) DNA were mixed in a 4:2:1 ratio. DNA/PEI mixtures were incubated at room temperature for 10 to 15 min, prior to application on HEK293-FTs. 24 and 48 h later, virus containing supernatant was harvested and filtered (0.45 µM). Virus was extracted using Lenti-X concentrator (Clontech Takara) according to the manufacturer's instructions. The virus containing pellet was resuspended in serum-free neurobasal medium and target cells were infected in the presence of 1 µg/ml polybrene (Sigma Aldrich). Two days following infection, cells were selected by growth in puromycin (E2 and G1 GSC: 1 µg/ml, G7 GSC: 0.5 µg/ml, Sigma) containing medium. Drug resistant E2 and G7 GSC were further sorted by FACS to isolate the high signal expressing population of iRFP-labelled GSC prior to intracranial implantation. iRFP positivity of G1 GSC iRFP was confirmed by FACS (Supplemental Fig. 2a).

Cell proliferation and cell viability assay. GSC were seeded in three wells of a 6-well plate at a density of 5×10^4 cells per well. Cell number for each well was assessed using a haemocytometer 1, 3 and 6 days after seeding. A median was calculated for each time point. Cell count was normalised to day 1 (n = 3 independent repeats per cell line).

Cell death and cell confluence were determined using live-cell imaging in the IncuCyte Zoom (Sartorius). Therefore, 12×10^3 GSC per well were seeded in 96-well plates and treated with the described chemotherapeutic agents in the presence of 30 nM SYTOX Green (Life Technologies). Plates were applied to the IncuCyte imager at 37 °C in a humidified 95% air/ 5% CO_2 incubator. Over a period of 48 h, every hour two images were taken per well. Images were presented in green phase contrast at 10 × magnification and quantified using IncuCyte imaging analysis software (Sartorius). The following drugs were used: ABT737 (ApexBio, A8193), S63845 (Chemgood, C-1370), Actinomycin D (Calbiochem, 114666), Temozolomide (Sigma, T2577), Cisplatin (Selleck, S1166), Paclitaxel (Sigma, T7191). Percentage cell death was calculated by normalising against maximal cell death following treatment with 1 µM Actinomycin D, 10 µM ABT737 and 1 µM S63845 (100% cell death control, verified by visual inspection of IncuCyte images) (n = 3 independent repeats per cell line).

Cell migration assay. For migration assays, 6-well plates were coated with gelatine, subsequently cross-linked with glutaraldehyde, quenched and equilibrated in serum-free GSC medium. GSC were seeded at a density of 8×10^4 per well, left to adhere and their movement was assessed over a 16-h period taking images every 10 min using time-lapse video microscopy and manual cell tracking software (Fiji). For cell migration assays, three independent repeats per cell line were performed and 60 cells per repeat were manually tracked and quantified using the chemotaxis plugin (Fiji).

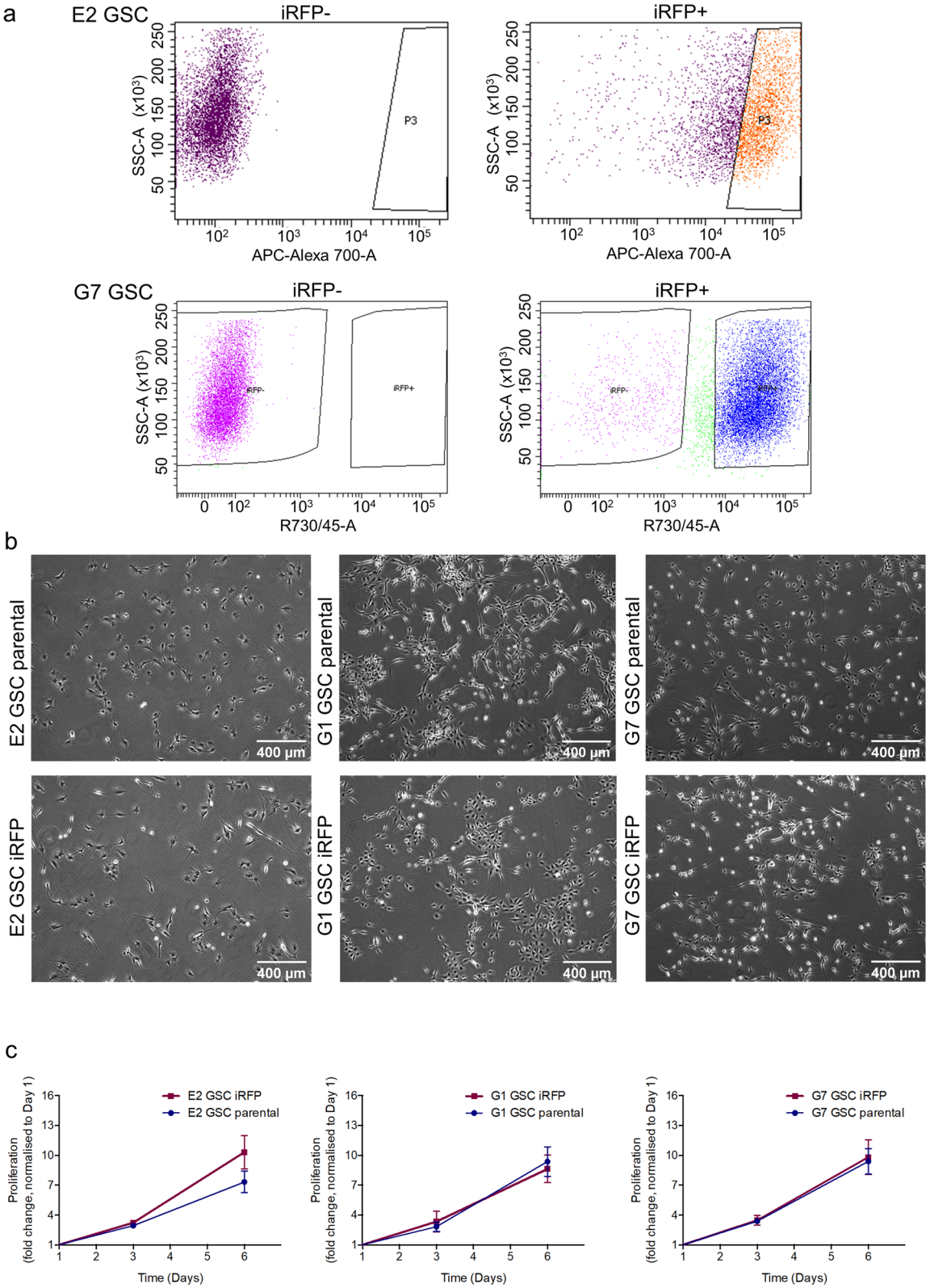

Figure 1. Generation of iRFP-expressing glioblastoma stem-like cells. (**a**) Flow cytometric plots showing sorting for higher signal iRFP-overexpressing E2 and G7 GSC (upper panel: P3 = high signal iRFP positive cells; lower panel: iRFP + = iRFP positive cells) (**b**) Representative images of monolayer E2, G1 and G7 GSC parental (upper panel) and iRFP-expressing cells (lower panel), respectively. (**c**) Proliferation assay of E2, G1 and G7 GSC counted at the indicated times after plating. Cell count was normalised to day 1. Error bars represent mean ± SD from n = 3 independent experiments.

Figure 2. iRFP-expressing GSC retain stem-like features. (**a**) Representative images of neurosphere growth from E2, G1 and G7 GSC parental (upper panel) and iRFP-expressing cells (lower panel), respectively. Quantification of neurosphere formation capacity by E2 parental vs. iRFP GSC ($p = 0.059$), G1 parental versus iRFP GSC ($p = 0.6427$) and G7 parental versus iRFP GSC ($p = 0.419$). Error bars represent mean ± SEM from n = 3 independent experiments; ns, nonsignificant. (**b**) Immunoblotting for cell-line specific neural stem cell markers (SOX2, OLIG2, Nestin) and astrocyte lineage differentiation marker GFAP in E2, G1 and G7 GSC parental compared with paired iRFP GSC, respectively. Alpha-tubulin served as loading control. Representative loading controls given (E2 GSC: membrane for SOX2/Nestin, G1 GSC: membrane for GFAP, G7 GSC: membrane for GFAP). All loading controls are displayed with full-length blots in Supplemental Figure 1. (**c**) Random cell migration assay from E2, G1 and G7 GSC parental and iRFP-expressing GSC on cross-linked gelatine. Values are mean ± SEM. n = 180 cells per cell line, ns, nonsignificant (E2 GSC parental vs E2 GSC iRFP: $p = 0.9189$, G1 GSC parental vs. G1 GSC iRFP: $p = 0.3625$ G7 GSC parental vs. G7 GSC iRFP: $p = 0.0650$). (**d**) E2, G1 and G7 GSC parental and iRFP-expressing GSC treated with indicated drugs for 48 h and analysed for cell viability using an IncuCyte imager and SYTOX Green exclusion. Percentage cell death was calculated by normalising against maximal cell death (48 h-treatment with 1 μM Actinomycin D, 10 μM ABT737 and 1 μM S6384). Error bars represent mean ± SEM from n = 3 independent experiments. No significant difference in response to treatment for all drugs tested in parental vs. iRFP matched counterparts (E2 GSC parental vs. E2 GSC iRFP: $p \geq 0.5186$, G1 GSC parental vs. G1 GSC iRFP: $p \geq 0.1072$, G7 GSC parental vs. G7 GSC iRFP: $p \geq 0.4302$).

Neurosphere formation assay. GSC were seeded in uncoated 96-well plates at a density of 10 cells per well. Medium was refreshed every week. Spheres were left to grow for 14 days (G1 and G7 GSC) or 21 days (E2 GSC) before manual scoring of the 60 inner wells (n = 3 independent repeats per cell line).

Immunoblotting and antibodies. GSC were initially lysed and collected in RIPA buffer (50 mM Tris-HCl pH 7.5, 150 mM NaCl, 1 mM EDTA, 1% NP-40), supplemented with Complete Protease Inhibitor (Roche) and PhosSTOP (Roche). Pierce BCA protein assay kit (Thermo Fisher Scientific) was used to determine protein concentration. Western blotting was performed by electrophoresis using 4–12% NuPage Bis-Tris protein gels (Thermo Fisher Scientific) followed by transfer to nitrocellulose membranes. After blocking in 5% non-fat dry milk, membranes were probed with primary antibodies (1:1,000 unless otherwise stated; SOX2 (Abcam #ab92494), Nestin (Abcam #ab22035), OLIG2 (R&D Systems #AF2418), GFAP (Santa Cruz #SC-6170) at 4 °C overnight. All membranes were incubated with α-tubulin serving as loading control (Sigma #T5168, 1:5,000) for one hour at room temperature. Membranes were incubated with Li-Cor secondary antibodies (IRDye 680RD donkey anti-mouse, IRDye 800CW donkey anti-rabbit, IRDye 800CW donkey anti-goat) for one hour at room temperature. Blots were imaged using Li-Cor Odyssey CLx (Li-Cor), acquired and processed using Image-Studio software (Li-Cor) and subsequently arranged using Adobe Illustrator.

Intracranial xenografts. All mouse experiments were carried out in accordance with the Animals Act 1986 (Scientific Procedures on living animals) and the regulatory guidelines of the EU Directive 2010 under project licences PPL PB6CB58C4 and P4A277133 and ethical review (University of Glasgow). 7-week old, female CD1-nude mice (Charles River, UK) were orthotopically injected with 1×10^5 iRFP-labelled or unlabelled E2 GSC or G7 GSC into the right striatum. Mice were monitored for the duration of the experiment and humanely sacrificed when they showed neurological (hemiparesis, paraplegia) or general symptoms (hunched posture, reduced mobility, and/or weight loss > 20%). To examine intracranial tumour growth in animals bearing iRFP-positive tumour cells, mice were monitored by PEARL imaging (Li-Cor) acquired and processed using Image-Studio software (Li-Cor). For imaging, mice were anaesthetised using isoflurane. Four weeks after tumour injection, a baseline scan was performed. Regular imaging was commenced 6 weeks (G7 GSC) or 8 weeks (E2 GSC) after tumour injection. The percentage change in the iRFP signal as a function of baseline scan was calculated according to the following equation:

$$\left(\frac{newIRFPsignal - baselineiRFPsignal}{baselineiRFPsignal}\right) * 100.$$

Immunohistochemistry and in situ hybridisation. H&E staining and immunohistochemistry (IHC) for Ki67 (Abcam #ab16667) and SOX2 (Abcam #ab92494) were performed on formalin-fixed, paraffin embedded brain sections (4 μm thick slices). For SOX2 IHC epitope retrieval was achieved by heating to 98 °C in pH6 citrate buffer for 60 min before proceeding as per the manufacturer's instructions with SOX2 antibody used at a dilution of 1:600 for E2 GSC and 1:400 for G7 GSC.

In situ hybridisation (ISH) analysis was performed using the RNAscope 2.5 LS (Brown, #322100) detection kit (Advanced Cell Diagnostics) on a Leica Bond Rx autostainer strictly adhering to manufacturer's instructions. To selectively identify human cells, a human-specific PPIB-probe (Hs-PPIB, Advanced Cell Diagnostics, #313908) was used. Scanning and image analysis of both was conducted using Leica SlidePath and Halo (Indica Labs). Algorithms were optimised for each stain individually and automated, quantitative analysis undertaken with Halo software (Indica Labs).

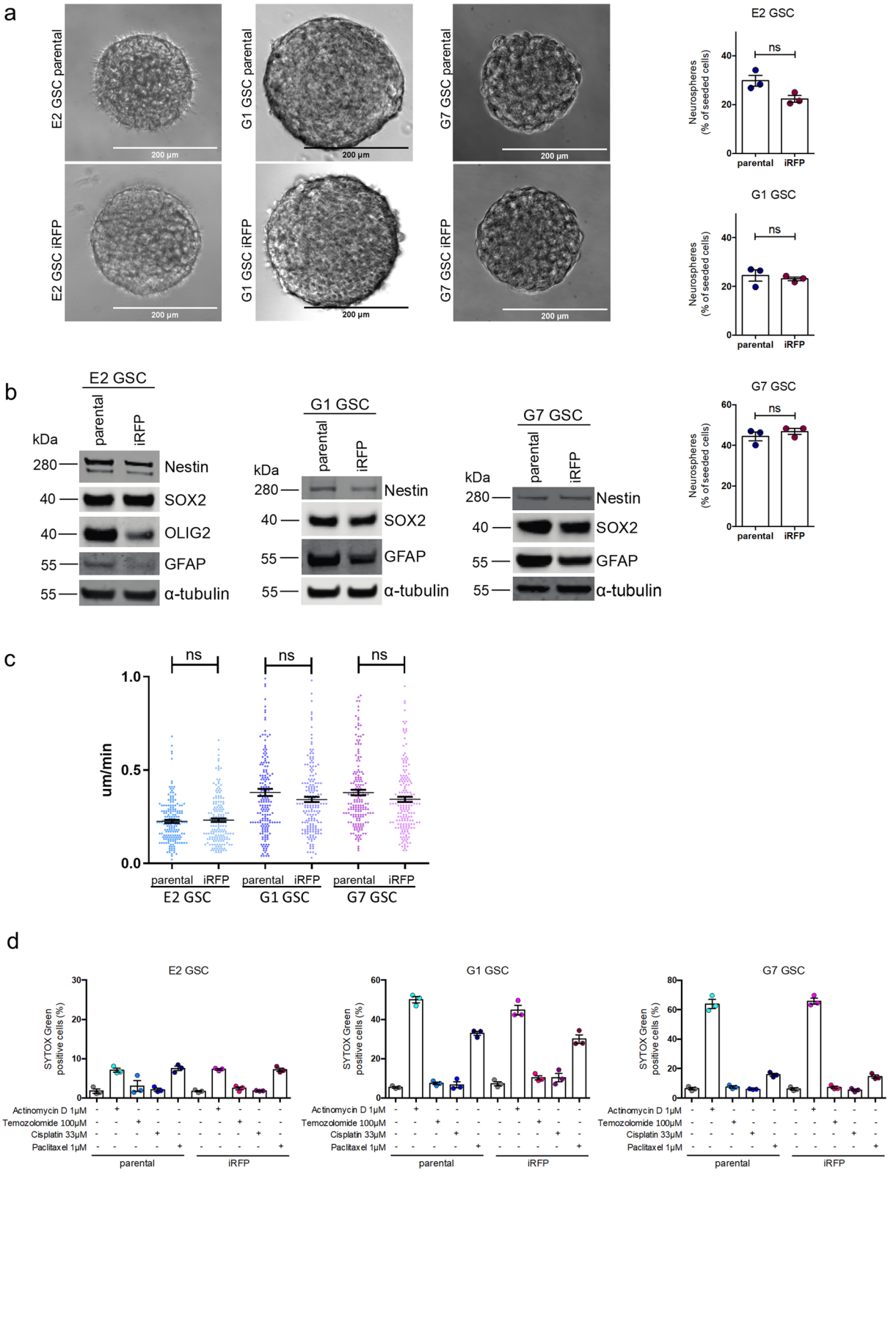
a
E2 GSC parental
G1 GSC parental
G7 GSC parental
E2 GSC iRFP
G1 GSC iRFP
G7 GSC iRFP
200 µm
E2 GSC
G1 GSC
G7 GSC
Neurospheres (% of seeded cells)
ns
parental
iRFP
b
kDa
Nestin
SOX2
OLIG2
GFAP
α-tubulin
c
um/min
parental
iRFP
d
SYTOX Green positive cells (%)
Actinomycin D 1µM
Temozolomide 100µM
Cisplatin 33µM
Paclitaxel 1µM

Statistical analyses. All statistical analyses were executed with Prism Software version 8.4.2 (GraphPad, La Jolla, CA, USA). Significance of neurosphere formation and cell viability assays was calculated using Welch's t-test. Significance of random cell migration assay was assessed using Mann–Whitney Test. For analysis of correlation of Ki67 positivity, Hs-PPIB positivity and iRFP signal increase, single linear regression and Spearman's *r* were used.

Results

Generation of iRFP-expressing glioblastoma stem-like cells. Near-infrared fluorescent proteins (iRFP) with excitation and emission in the 700 and 800 nm spectra allow tumour detection in deep tissues with only minimal interference from tissue autofluorescence[11]. Since the use of iRFP in mouse models was first described in 2011, it has been shown to be a powerful and reliable tool to measure cell proliferation in vitro and in vivo[11,14]. We deployed a retroviral transduction approach to express iRFP in E2, G1 and G7 GSC, three primary patient-derived cell lines originally derived from fresh patient tissue as previously described[12,13]. We tailored the protocol to reduce the number of manipulations so as to minimise effects on the heterogeneous nature of the GSC cultures. To avoid culturing GSC in FCS containing medium, which would drive cell differentiation, the iRFP-encoding retroviruses were resuspended in neurobasal medium. 48 h after infection, enrichment of iRFP-expressing GSC was commenced using puromycin selection. Cell lines used for intracranial injections were further sorted for a cell population with higher signal intensity using fluorescence activated cell sorting (FACS) (Fig. 1a). Due to the infiltrative nature of E2 GSC xenograft growth, stricter gating parameters were applied to ensure subsequent detectability of the iRFP signal in vivo. There were no detectable differences between the morphology and proliferation rates of iRFP-expressing GSC and their matching parental controls (Fig. 1b,c).

iRFP-expressing GSC retain stem-like features. Cancer stem cells are understood to be the tumourigenic drivers of glioblastoma[15–17]. Consequently, extensive research has been devoted to refining glioblastoma culturing methods so as to preserve the specific stem-like properties of patient tumour specimens[9,12,15,18]. The microenvironment, including medium composition and culture conditions, inevitably affect the characteristics of stem cell populations[19]. Their self-renewal capacity not only encourages rapid adaption to alterations in the microenvironment, but can also drive resistance to cancer therapies[20]. Thus, we were keen to determine whether changes in stem cell characteristics had occurred after retroviral transduction. The capacity to form neurospheres (as a proxy for tumour initiation) was conserved in the iRFP-expressing GSC, although a slight (but not statistically significant) decrease of neurosphere forming capacity was detectable in the E2 GSC iRFP (Fig. 2a). Furthermore, the expression of cell lineage-specific neural stem cell (SOX2, Nestin, OLIG2) and astrocytic differentiation (GFAP) markers was maintained upon retroviral transduction and expression of iRFP, despite a moderate decrease in OIG2 and GFAP protein levels in E2 GSC (Fig. 2b). To investigate the migratory behaviour of iRFP-labelled GSC in comparison to their parental counterpart we deployed a random cell migration assay. No significant changes in cell migratory speed could be detected between the corresponding cell lines (Fig. 2c). Furthermore, we interrogated whether the cell-line specific cytostatic and cytotoxic response to a panel of standard chemotherapeutic agents was maintained (Fig. 2d, Supplemental Fig. 2b). We found that iRFP-labelled primary GSC retain a comparable level of resistance to established chemotherapeutics. Taken together, these data demonstrate that our approach to achieve iRFP expression is unlikely to influence GSC stem-like behaviour and response to treatment.

Quantitative imaging of iRFP-expressing glioblastoma in vivo. We next determined whether iRFP was suitable for measuring glioblastoma growth in vivo. For this purpose, we generated orthotopic xenografts using E2 GSC iRFP and G7 GSC iRFP. When implanted into the right striatum of 7-week old CD1-nude mice, both iRFP-expressing cell lines retained the growth pattern characteristics and SOX2 expression of their parental counterparts (Supplemental Fig. 3a,b). While iRFP-expressing G7 GSC grew mainly as a solid tumour with invasive margins, E2 GSC iRFP disseminated throughout the brain as widely scattered tumour cells (formerly described as gliomatosis cerebri) to such an extent that the presence of a solid tumour at the injection site was not readily discernible (Fig. 3a). To date, no imaging tool has been capable of reliably detecting or quantitatively monitoring growth of highly invasive tumour xenografts, such as those engendered by E2 GSC. To determine whether iRFP expression enabled bona fide quantification of these highly disseminated tumours, we implanted 1×10^5 iRFP-expressing E2 GSC into nude mice as before. Mice were initially scanned using a PEARL imager to establish a baseline, and this was performed 4 weeks after surgery to allow for sufficient recovery and wound healing. Images from single mice were acquired within 30s, followed by a short awakening and recovery phase. Based on previous studies using E2 GSC, we began imaging the mice at regular intervals from week 8 until clinical endpoint or 31 weeks after surgery[21,22]. Analysis of the signal intensity over time revealed that a measurable increase in signal (with reference to the 4 week baseline) was detected as early as 16 weeks after surgery, delineating individual rates of signal increase for each animal (Fig. 3b,c). To investigate the utility of iRFP imaging in PDX models growing as solid tumours with invasive margins, we used orthotopic G7 iRFP GSC xenografts. In this experiment, imaging commenced six weeks after tumour cell injection. Individual signal increase patterns for each of the three mice were detectable from 8 weeks following implantation, thus indicating that iRFP-expressing GSC may be used to monitor the growth of glioblastoma PDXs over an extended time course (Fig. 3d,e).

iRFP signal correlates with histological tumour burden. To determine whether the fluorescent signal emanating from iRFP-expressing GSC tumours correlated with histological tumour burden, we imaged brains bearing G7 GSC iRFP xenografts. We then fixed these brains ex vivo and stained them using H&E, thus

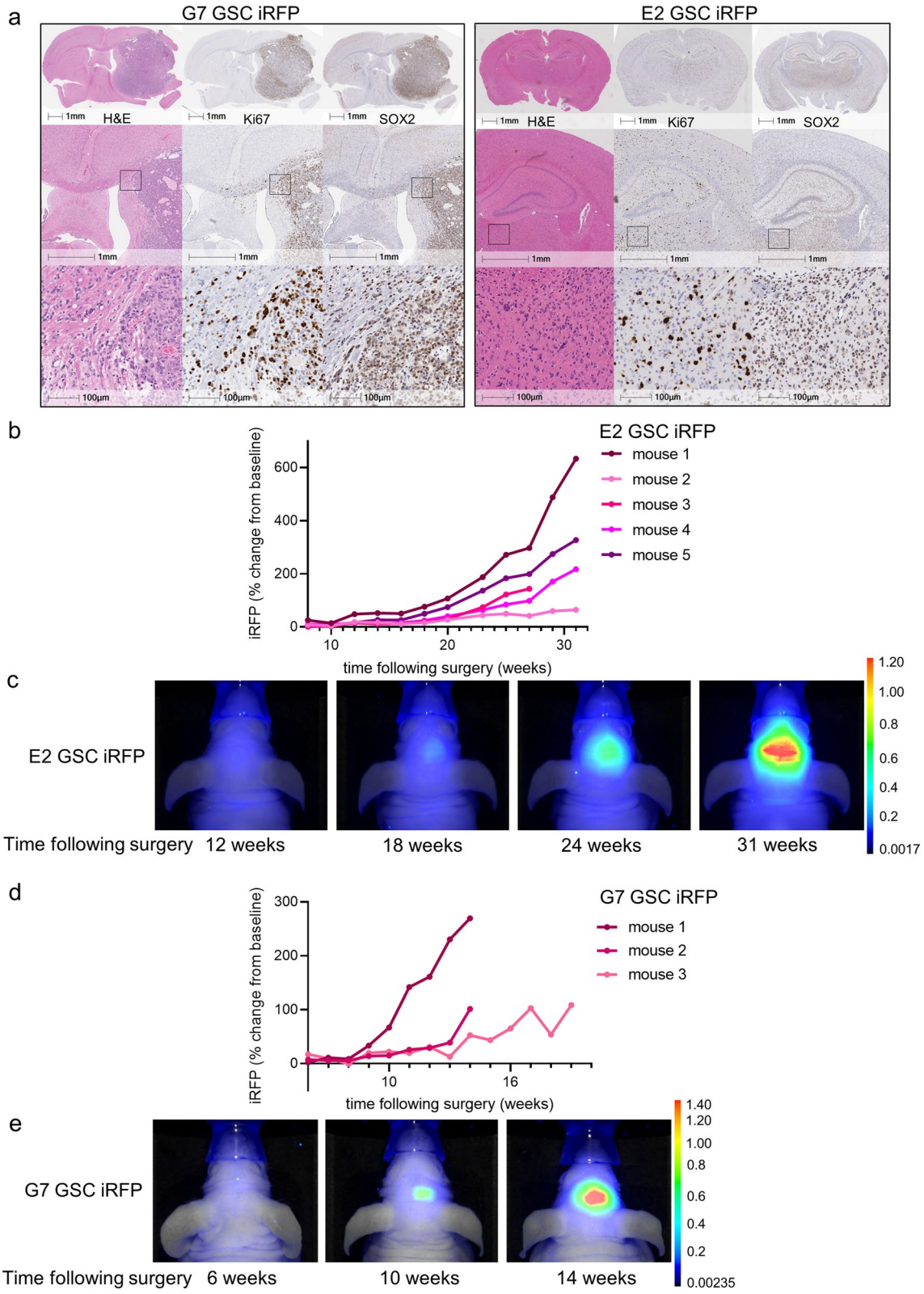

Figure 3. Quantitative imaging of iRFP-expressing glioblastoma in vivo. (**a**) Representative images of haematoxylin and eosin (H&E), Ki67 and SOX2 immunohistochemistry of brain sections containing orthotopic tumours derived from intracranially injected G7 or E2 GSC iRFP. (**b**) E2 GSC iRFP were injected intracranially into five mice. iRFP signal increase was measured at indicated times (**c**,**e**). Pseudocolour representations of iRFP signal increase over time in individual mice bearing E2 or G7 GSC iRFP tumours, respectively, as detected by PEARL scans (700 nm channel). (**d**) G7 GSC iRFP were injected intracranially in three mice. iRFP signal increase measured at indicated times.

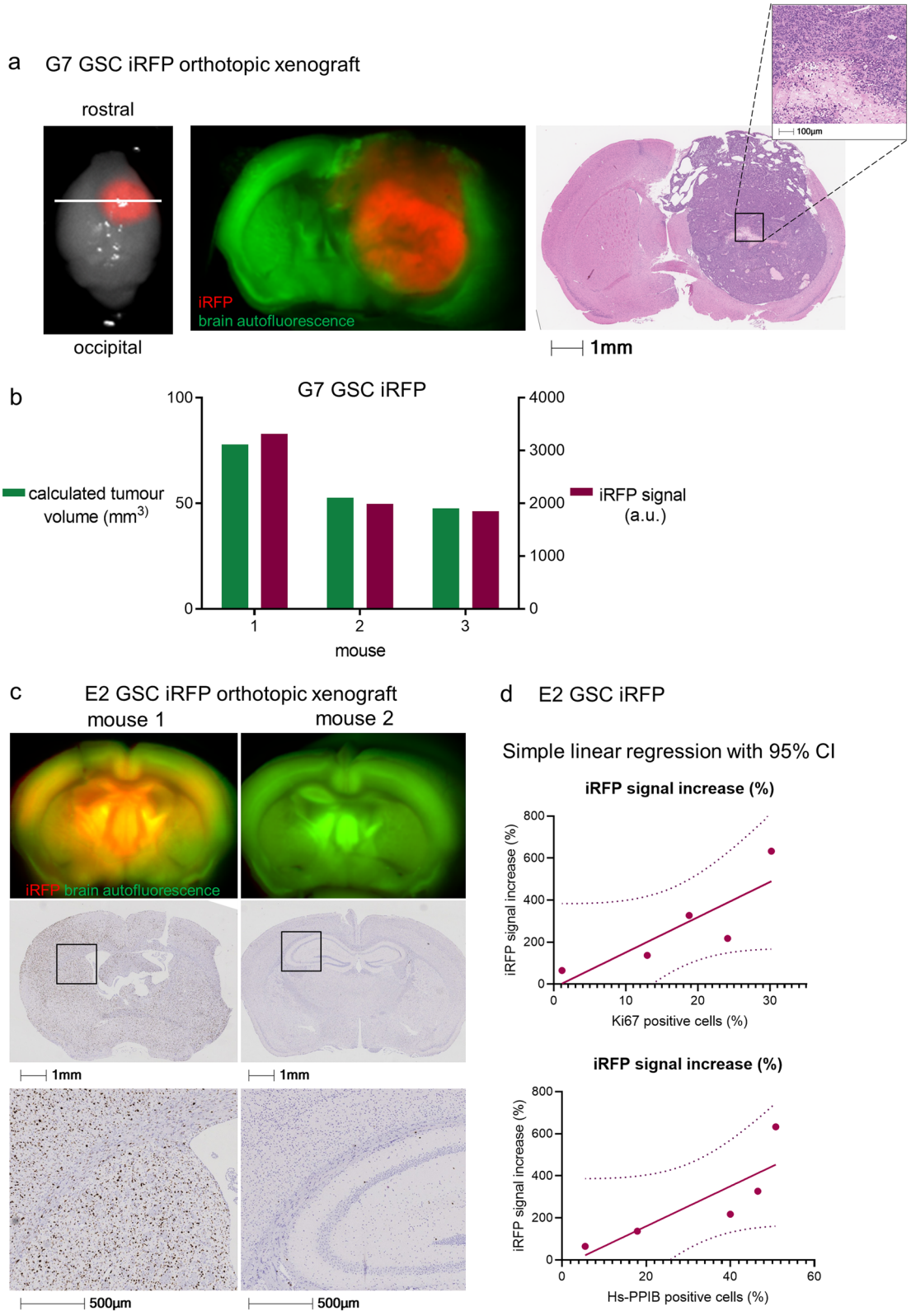

Figure 4. iRFP signal correlates with histological tumour burden. (**a**) Representative ex vivo PEARL and Odyssey scans of G7 GSC iRFP tumour in a mouse brain after resection (left), and on coronar section (middle, denoted by white line in left image) in comparison to matching H&E stain (right). 700 nm scan (red) was used to visualise the tumour, brain autofluorescence was detected in 800 nm channel (green). (**b**) G7 GSC iRFP signal detected with PEARL imager (a.u., arbitrary units) corresponds with calculated spherical tumour volume (mm^3), extrapolated from mean diameter in H&E stains. (**c**) Upper panel: Odyssey scans of coronar sections from E2 GSC iRFP bearing mice. 700 nm scan (red) was used to visualise tumours, brain autofluorescence was detected in 800 nm channel (green). Middle and lower panel: corresponding Ki67 staining and magnification. (**d**) Simple linear regression correlating E2 GSC iRFP signal with percentage of Ki67 positive tumour cells and Hs-PPIB-positive tumour cells in five mice, quantified with Halo analysis software (Ki67: $p = 0.0755$, Spearman correlation $r = 0.9$, Hs-PPIB: $p = 0.0773$, Spearman correlation $r = 1$).

allowing comparison of the fluorescence and histological fields. We found that in mice implanted with G7 GSC, iRFP fluorescence faithfully delineated the extent of intraparenchymal spread that had been detected using iRFP imaging. Strikingly, imaging was sufficiently sensitive to illustrate the central core necrosis that was evident following H&E staining (Fig. 4a). Since G7 iRFP tumours grew approximately spherically in vivo, we extrapolated tumour volume from the mean diameter in H&E and correlated it with the absolute iRFP signal measured at the final imaging obtained before endpoint. Notably, the fluorescent signal emanating from iRFP-expressing G7 GSC tumour bearing mice was highly concordant with the calculated tumour volume (Fig. 4b). As highly invasive models such as E2 GSC do not permit measurement of a defined tumour bulk, we sought to examine the accuracy with which iRFP signal intensity represented tumour burden. Using the proportion of Ki67-positive cells across the brain section as a proxy, we observed that the burden of disseminated E2 GSC tumour cells varied substantially between animals, similar to the intravital imaging data (Fig. 4c). Moreover, we found that the relative iRFP signal increase at endpoint correlated strongly with the relative prevalence of Ki67-positive cells (Spearman correlation $r = 0.9$) (Fig. 4d). To evaluate the robustness of this correlation, we conducted in situ hybridisation for human-specific PPIB. Affirmingly, we observed a strong correlation between the relative final iRFP signal increase and the relative prevalence of human-specific PPIB (Spearman correlation $r = 1$). Taking into account the limited number of animals, the observed trend towards statistical significance for both markers (Ki67: $p = 0.0755$, PPIB: $p = 0.0773$) supports the reliability of the model. In summary, our data demonstrate that near-infrared labelling of highly invasive primary patient-derived glioblastoma cells is a powerful tool to quantitatively monitor their growth in vivo.

Discussion

Reporter gene-based technologies, such as luciferase-based bioluminescence, are widely used but have particular limitations especially with regard to quantitative longitudinal assessment of tumour xenograft growth. In this paper we show that the use of cell lines stably expressing iRFP overcomes many of these limitations. We have demonstrated that it is feasible to manipulate primary glioblastoma stem-like cells by stably overexpressing the near-infrared fluorescent protein iRFP without overtly affecting their particular stem-like properties. Signal intensity is consistent and reliable over time and permits monitoring of orthotopic tumour growth in vivo with a high degree of accuracy. This is especially valuable for highly invasive cell lines such as E2 GSC, which cannot be detected or quantified with conventional imaging methods such as MRI. As iRFP enables cost-effective, repeated and comparatively high throughput non-invasive imaging of mice bearing orthotopic glioblastoma PDX, it could be used to determine individual treatment start dates for mice when they reach a certain threshold, mimicking more closely the clinical scenario. Additionally, this method may also be used to stratify mice into cohorts depending on their actual biological tumour burden. This application serves to reduce the number of mice needed for statistical power in heterogenous primary glioblastoma PDX-models.

Use of additional patient-derived PDX would help to further validate the general applicability of our model. A further advantage of iRFP expressing tumours is the ability to FACS-sort tumour cells without the need for antibody labelling, enhancing cell viability and leaving cell surface molecules unperturbed.

In summary, our results show that iRFP serves as a reliable and sensitive tool to monitor intracranial tumour growth in both highly invasive and more localised primary glioblastoma orthotopic xenograft models without affecting their phenotypes. This new technique provides significant benefits for the design, execution and analysis of in vivo studies using glioblastoma PDX.

Received: 15 May 2020; Accepted: 26 August 2020
Published online: 21 September 2020

References

1. Louis, D. N. *et al.* The 2016 World health organization classification of tumors of the central nervous system: a summary. *Acta Neuropathol.* **131**, 803–820. https://doi.org/10.1007/s00401-016-1545-1 (2016).
2. Ostrom, Q. T. *et al.* CBTRUS statistical report: primary brain and other central nervous system tumors diagnosed in the United States in 2012–2016. *Neuro Oncol.* **21**, v1–v100. https://doi.org/10.1093/neuonc/noz150 (2019).
3. Stupp, R. *et al.* Effects of radiotherapy with concomitant and adjuvant temozolomide versus radiotherapy alone on survival in glioblastoma in a randomised phase III study: 5-year analysis of the EORTC-NCIC trial. *Lancet Oncol.* **10**, 459–466. https://doi.org/10.1016/S1470-2045(09)70025-7 (2009).
4. Patrizii, M., Bartucci, M., Pine, S. R. & Sabaawy, H. E. Utility of glioblastoma patient-derived orthotopic xenografts in drug discovery and personalized therapy. *Front. Oncol.* **8**, 23. https://doi.org/10.3389/fonc.2018.00023 (2018).
5. Aldape, K. *et al.* Challenges to curing primary brain tumours. *Nat. Rev. Clin. Oncol.* **16**, 509–520. https://doi.org/10.1038/s41571-019-0177-5 (2019).
6. Pastrana, E., Silva-Vargas, V. & Doetsch, F. Eyes wide open: a critical review of sphere-formation as an assay for stem cells. *Cell Stem Cell* **8**, 486–498. https://doi.org/10.1016/j.stem.2011.04.007 (2011).
7. Lathia, J. D., Mack, S. C., Mulkearns-Hubert, E. E., Valentim, C. L. & Rich, J. N. Cancer stem cells in glioblastoma. *Genes Dev.* **29**, 1203–1217. https://doi.org/10.1101/gad.261982.115 (2015).
8. Lee, J. *et al.* Tumor stem cells derived from glioblastomas cultured in bFGF and EGF more closely mirror the phenotype and genotype of primary tumors than do serum-cultured cell lines. *Cancer Cell* **9**, 391–403. https://doi.org/10.1016/j.ccr.2006.03.030 (2006).
9. Pollard, S. M. *et al.* Glioma stem cell lines expanded in adherent culture have tumor-specific phenotypes and are suitable for chemical and genetic screens. *Cell Stem Cell* **4**, 568–580. https://doi.org/10.1016/j.stem.2009.03.014 (2009).
10. Claes, A. *et al.* Phenotypic and genotypic characterization of orthotopic human glioma models and its relevance for the study of anti-glioma therapy. *Brain Pathol.* **18**, 423–433. https://doi.org/10.1111/j.1750-3639.2008.00141.x (2008).
11. Hock, A. K. *et al.* iRFP is a sensitive marker for cell number and tumor growth in high-throughput systems. *Cell Cycle* **13**, 220–226. https://doi.org/10.4161/cc.26985 (2014).

12. Fael Al-Mayhani, T. M. *et al.* An efficient method for derivation and propagation of glioblastoma cell lines that conserves the molecular profile of their original tumours. *J. Neurosci. Methods* **176**, 192–199. https://doi.org/10.1016/j.jneumeth.2008.07.022 (2009).
13. Ahmed, S. U. *et al.* Selective inhibition of parallel DNA damage response pathways optimizes radiosensitization of glioblastoma stem-like cells. *Cancer Res.* **75**, 4416–4428. https://doi.org/10.1158/0008-5472.can-14-3790 (2015).
14. Filonov, G. S. *et al.* Bright and stable near-infrared fluorescent protein for in vivo imaging. *Nat. Biotechnol.* **29**, 757–761. https://doi.org/10.1038/nbt.1918 (2011).
15. Ignatova, T. N. *et al.* Human cortical glial tumors contain neural stem-like cells expressing astroglial and neuronal markers in vitro. *Glia* **39**, 193–206. https://doi.org/10.1002/glia.10094 (2002).
16. Cheng, L. *et al.* Glioblastoma stem cells generate vascular pericytes to support vessel function and tumor growth. *Cell* **153**, 139–152. https://doi.org/10.1016/j.cell.2013.02.021 (2013).
17. Singh, S. K. *et al.* Identification of human brain tumour initiating cells. *Nature* **432**, 396–401. https://doi.org/10.1038/nature03128 (2004).
18. Singh, S. K. *et al.* Identification of a cancer stem cell in human brain tumors. *Cancer Res.* **63**, 5821–5828 (2003).
19. Gilbertson, R. J. & Rich, J. N. Making a tumour's bed: glioblastoma stem cells and the vascular niche. *Nat. Rev. Cancer* **7**, 733–736. https://doi.org/10.1038/nrc2246 (2007).
20. Bao, S. *et al.* Glioma stem cells promote radioresistance by preferential activation of the DNA damage response. *Nature* **444**, 756–760. https://doi.org/10.1038/nature05236 (2006).
21. Gomez-Roman, N., Stevenson, K., Gilmour, L., Hamilton, G. & Chalmers, A. J. A novel 3D human glioblastoma cell culture system for modeling drug and radiation responses. *Neuro Oncol.* **19**, 229–241. https://doi.org/10.1093/neuonc/now164 (2017).
22. Mannino, M., Gomez-Roman, N., Hochegger, H. & Chalmers, A. J. Differential sensitivity of Glioma stem cells to Aurora kinase A inhibitors: implications for stem cell mitosis and centrosome dynamics. *Stem Cell Res.* **13**, 135–143. https://doi.org/10.1016/j.scr.2014.05.001 (2014).

Acknowledgements

We thank Professor Colin Watts for providing the E2, G1 and G7 GSC, Dr. Andreas Hock for providing the pBABE iRFP IRES puro construct and Dr. David Bryant for providing the HEK293-FT cells. In addition, we thank Tom Gilbey, Gemma Thomson, the Histology Service, Biological Services, and all Core Services at the CRUK Beatson Institute for their invaluable assistance. Many thanks to Dr. Matthew Neilson for his invaluable support and advice on statistical analysis, and Dr. Florian Bock and Dr. Catherine Winchester for critical reading and assistance in the preparation of this manuscript. This work was supported by CRUK core funding to the Beatson Institute (A17196) to C.N. and to J.C.N. (A18277), a CRUK Programme Foundation Award (C40872/A20145) to S.W.T., CRUK Clinical Research Fellowship to A.L.K. (A23220), funding by the University of Glasgow to D.K. and A.C, funding by Chief Scientist Office to N.G-R. (ETM/405) and funding by the Beatson Cancer Charity and Cancer Research UK RadNet Centre Glasgow to K.S.

Author contributions

A.L.K. and D.K. performed experiments. K.S., C.C., C.N. and L.M. provided assistance with the intracranial xenograft model and related imaging. N.G-R. provided histology samples of intracranial xenografts of parental cell lines. A.L.K. and D.K. designed experiments and analysed the data. A.L.K., D.K., S.W.G.T. and J.C.N. wrote the manuscript. A.C., S.W.G.T. and J.C.N. directed the study.

Competing interests

The authors declare no competing interests.

Additional information

Supplementary information is available for this paper at https://doi.org/10.1038/s41598-020-72322-x.

Correspondence and requests for materials should be addressed to J.C.N. or S.W.G.T.

Reprints and permissions information is available at www.nature.com/reprints.

Publisher's note Springer Nature remains neutral with regard to jurisdictional claims in published maps and institutional affiliations.